

**Shining Light on Dark Matter,  
One Photon at a Time**

by

Brandon Leigh Allen

Submitted to the Department of Physics  
in partial fulfillment of the requirements for the degree of

Doctorate of Science in Physics

at the

MASSACHUSETTS INSTITUTE OF TECHNOLOGY

June 2019

© Massachusetts Institute of Technology 2019. All rights reserved.

Author .....  
Department of Physics  
May 18, 2019

Certified by .....  
Christoph E.M. Paus  
Professor  
Thesis Supervisor

Accepted by .....  
Nergis Mavalvala  
Associate Department Head for Education



**Shining Light on Dark Matter,  
One Photon at a Time**

by

Brandon Leigh Allen

Submitted to the Department of Physics  
on May 18, 2019, in partial fulfillment of the  
requirements for the degree of  
Doctorate of Science in Physics

**Abstract**

A search is conducted for new physics in final states containing a photon and missing transverse momentum in proton-proton collisions at  $\sqrt{s} = 13$  TeV. The data collected by the CMS experiment at the CERN LHC correspond to an integrated luminosity of 35.9 inverse femtobarns. No deviations from the predictions of the standard model are observed. The results are interpreted in the context of dark matter production and limits on new physics parameters are calculated at 95% confidence level. For the two simplified dark matter production models considered, the observed (expected) lower limits on the mediator masses are both 950 (1150) GeV for 1 GeV dark matter mass.

Thesis Supervisor: Christoph E.M. Paus

Title: Professor



## Acknowledgments

This is the acknowledgements section. You should replace this with your own acknowledgements.



# Contents

<b>1</b>	<b>Dark Matter</b>	<b>9</b>
1.1	Astrophysical Evidence . . . . .	10
1.1.1	Galactic Clusters . . . . .	10
1.1.2	Galactic Rotation Curves . . . . .	11
1.1.3	Gravitational Lensing . . . . .	12
1.1.4	Cluster Collisions . . . . .	13
1.2	Relic Density . . . . .	16
1.3	Dark Matter Candidates . . . . .	18
1.3.1	Weakly-Interacting Massive Particles . . . . .	19
1.3.2	Axions . . . . .	19
1.3.3	Sterile Neutrinos . . . . .	20
1.4	Simplified Models for LHC . . . . .	22
1.5	Non-collider Searches . . . . .	24
1.5.1	Direct Detection . . . . .	24
1.5.2	Indirect Detection . . . . .	27
1.6	Summary . . . . .	29



# Chapter 1

## Dark Matter

As a theory of the fundamental particles and forces of nature, the Standard Model should also help explain physics at the largest scales. The  $\Lambda$ CDM model [1] best explains all current cosmological observations including the structure of the cosmic microwave background; the abundances of hydrogen, helium, and lithium; the large-scale structure in the distribution of galaxies, and the accelerating expansion of the universe. However, results from many cosmological observations show that baryonic matter (matter consisting of various combinations of protons, neutrons, and electrons) only contributes  $\sim 5\%$  of the total energy of the universe, with radiation (photons and relativistic neutrinos) contributing less than a hundredth of a percent.

The remaining 95% of energy comes from just two sources:  $\sim 27\%$  from non-relativistic non-baryonic matter referred to as dark matter and  $\sim 68\%$  from an unknown form of energy that permeates all of space referred to as dark energy. Current observations show that dark energy is uniform in space and time producing a similar effect to that of the cosmological constant in the Einstein field equations of general relativity. Not much else is known about dark energy, although there are many experiments attempting to discover additional properties. The work in this thesis shall focus on trying to explain dark matter.

Dark matter cannot be explained by the 17 particles of the Standard Model, yet its gravitational effects have been observed in many circumstances. The rest of this chapter will cover the astrophysical evidence for dark matter (Sections 1.1 and 1.2),

various dark matter candidates (Section 1.3) and the models investigated at the LHC (Section 1.4), and non-collider searches for dark matter (Section 1.5).

## 1.1 Astrophysical Evidence

All existing evidence for dark matter comes from astrophysical observations of its gravitational effects on the universe at various length scales. We shall focus on four different sources of evidence: the average velocity of galaxies in clusters, the rotation curves of spiral galaxies, strong gravitational lensing, and merging galactic clusters. The evidence presented here is not exhaustive, see Reference [2] for more detail.

### 1.1.1 Galactic Clusters

Galactic clusters are the largest gravitational bound systems, with the orbital velocities of the individual clusters determined by the total gravitational mass of the cluster. Applying the Virial Theorem gives the explicit relation

$$v^2 = \frac{GM}{2r}, \quad (1.1)$$

where  $v$  is the average orbital velocity of a galaxy in the cluster,  $r$  is the average separation between galaxies in the cluster,  $M$  is the total gravitational mass of the cluster, and  $G$  is the Newtonian constant of gravitation. In 1933, Fritz Zwicky measured the average orbital velocity of the Coma cluster and using Equation 1.1 calculated that its mass was a factor of ten larger than the observed visible mass, leading to the conclusion that the majority of the cluster consisted of non-luminous matter [3]. Today studies show that stars only contribute 1% of the total cluster mass, with a hot, baryonic intracluster medium and dark matter contributing the remaining 14% and 85% of the total cluster mass, respectively [2].

### 1.1.2 Galactic Rotation Curves

Spiral galaxies are stable gravitational bound systems with stars and interstellar gas rotating around the galactic center in nearly circular orbits in a single plane. For these galaxies, the orbit of an individual star is stable when the gravitational force acting on the star balances the centripetal acceleration of the star. With this condition, the expected stellar velocity  $v$  is a function of distance  $r$  from the galactic center given by

$$v = \sqrt{\frac{GM(r)}{r}}, \quad (1.2)$$

where  $M(r)$  is the total gravitational mass inside radius  $r$ . Thus, past a certain critical radius  $r_c$ , the stellar velocity should fall with as  $r^{1/2}$  as the mass of the galaxy is no longer increasing significantly [4].

In 1980, Vera Rubin and Kent Ford observed that instead of decreasing at distances outside the visible galaxy, the stellar velocity stayed constant out to a very great distance, necessitating an additional non-luminous source of mass [5]. The most common explanation for this missing mass is the existence of an isotropic dark matter halo surrounding the galaxy. With the inclusion of interstellar gas, the total mass inside radius  $r$  is given by

$$M(r) = 4\pi \int_0^r dr' (r')^2 [\rho_S(r') + \rho_g(r') + \rho_{DM}(r')], \quad (1.3)$$

where  $\rho_S$ ,  $\rho_g$ , and  $\rho_{DM}$  are the density profiles of the stars, interstellar gas, and dark matter in the galaxy, respectively. Once these densities have been specified, it is possible to plot the fraction of the total stellar velocity due to each mass source as a function of distance from the galactic center. Figure 1-1 shows the results of doing this using the observed stellar and interstellar mass density profiles and the expected density from an isotropic dark matter halo for two different spiral galaxies. In both cases, this reproduces the observed flat galactic rotation curve incredibly well, lending strong support for the existence of galactic dark matter halos.

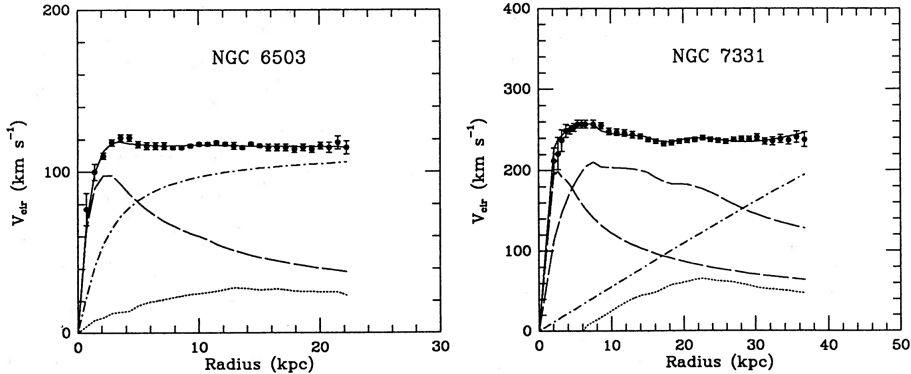


Figure 1-1: The observed (points) and fitted (solid line) rotation curves for two sample galaxies. The fit consists of three components: the stellar component (dashed), the interstellar gas (dotted), and the dark matter halo (dash-dotted). Reprinted from Reference [6].

### 1.1.3 Gravitational Lensing

As a consequence of Einstein's equivalence principle, a massive body will deflect light, a phenomenon known as gravitational lensing. In the language of general relativity, this means that the photons take the path given by the geodesic lines following the curvature of space-time due to the massive body. For most observations of gravitational lensing due to astrophysical bodies, the physical size of the lensing object is much smaller than the distance between observer, lens, and source allowing us to use the thin lens approximation. Approximating the lens as a planar distribution of matter, the angular deflection is given by

$$\vec{\alpha}(\vec{x}) = \frac{4G}{c^2} \int d^2x' \frac{\vec{x} - \vec{x}'}{|\vec{x} - \vec{x}'|^2} \int dz \rho(\vec{x}', z) \quad (1.4)$$

where  $\vec{x}$  is a two-dimensional vector in the plane of the lens,  $z$  is the perpendicular distance from the plane of the lens, and  $\rho$  is the three dimensional density [7]. If the source is treated as a point mass, this reduces to

$$\alpha = \frac{4G}{c^2} \cdot \frac{M}{b} \quad (1.5)$$

where  $b = |\vec{x} - \vec{x}'|$  is the impact parameter and  $M$  is the total mass of the object. Thus, measuring the angle of deflection due to gravitational lensing around an astrophysical object provides an independent measurement of the total mass of the body which can be compared to the mass of the luminous objects in the body.

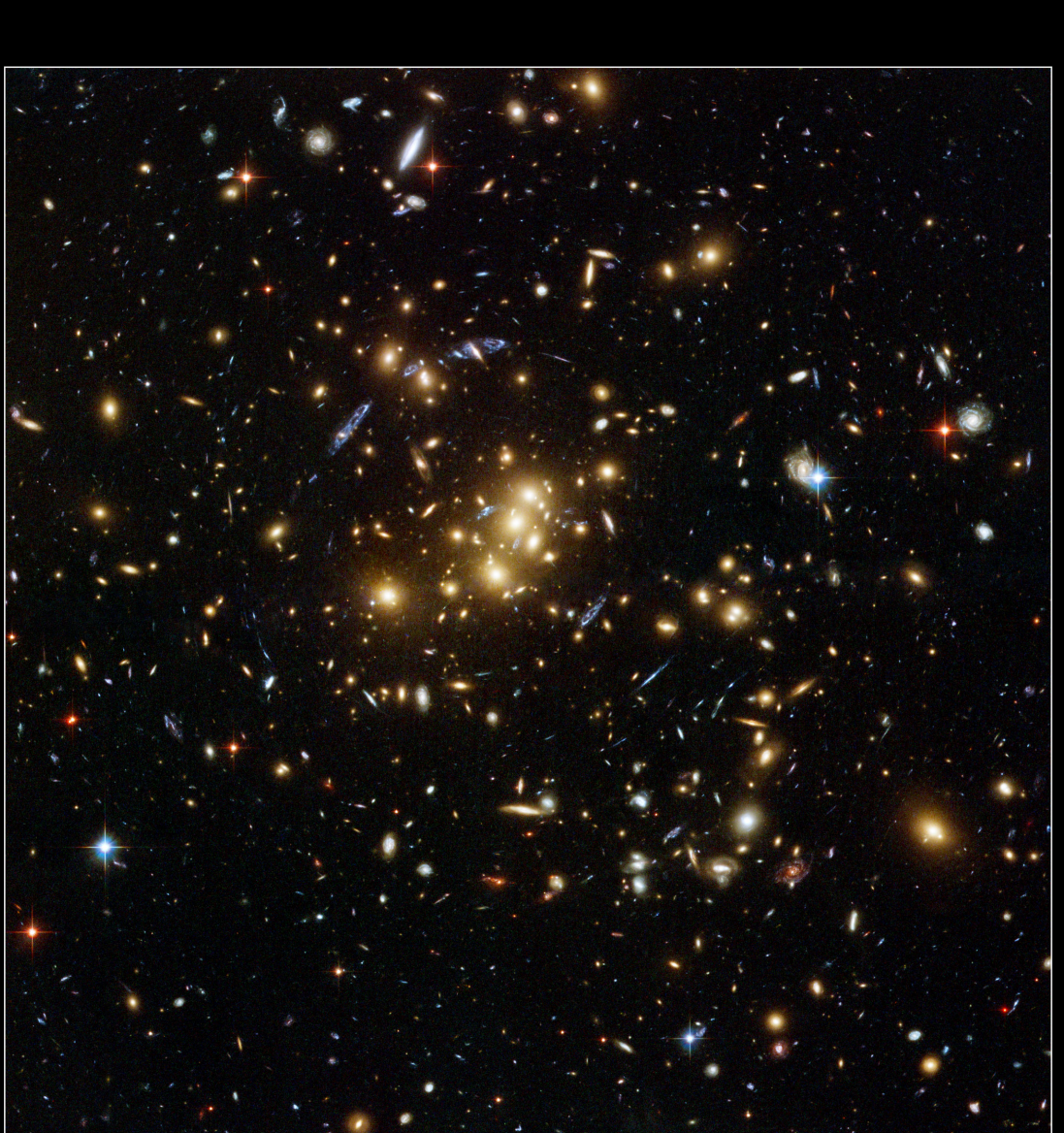
Depending on the mass of the deflecting body and impact parameter, the size of deflection can fall into three different regimes. The first of these is called strong lensing where the curving of space-time is so strong that light can travel multiple paths around the lens and still reach the observer. If the source is directly behind a circular lens, light travels around all sides of the lens and appears as an Einstein ring, while if the source is offset or the lens is non-circular, the source will instead appear in multiple locations as if viewed from slightly different angles. An example of strong lensing is shown in Figure 1-2.

The next regime is known as weak lensing, where the deflection is enough to distort the image of the source but not enough to result in multiple images. The shear of this distortion can be converted into a map of the projected mass distribution. True weak lensing results in circular “*E-mode*” patterns while sources of systematic uncertainty produce both “*E-mode*” and curl-like “*B-mode*” patterns. Thus, requiring a zero “*B-mode*” contribution assures that the measured mass distribution is accurate. Figure 1-3 shows the observed shear of half a million galaxies measured in the Hubble Space Telescope COSMOS survey.

The final regime is the microlensing that occurs when a lens moves relative to a luminous source. As the lens passes in front of the source, it will temporarily increase the apparent luminosity of the source, enabling a mass measurement of the lens. Microlensing results show that rocky exoplanets orbit other stars and that these planets cannot form the bulk of dark matter in the Milky Way.

#### 1.1.4 Cluster Collisions

Gravitational lensing measurements of galactic cluster collisions provide support for dark matter and help constrain its properties. Figure 1-4 shows the merging cluster 1E0657-558. By comparing the weak lensing reconstruction of the gravitational po-



**Galaxy Cluster Cl 0024+17 (ZwCl 0024+1652)**  
*Hubble Space Telescope • ACS/WFC*

NASA, ESA, and M.J. Jee (Johns Hopkins University)

STScI-PRC07-17b

Figure 1-2: Strong gravitational lensing around galaxy cluster CL0024+17, consisting of the gravitationally bound yellow, elliptical galaxies. The elongated blue objects are from much more distant galaxies behind the cluster which are distorted into arcs due to gravitational lensing from the dark matter halo surrounding the cluster. Figure credit: NASA, ESA, M.J. Jee and H. Ford (Johns Hopkins University)

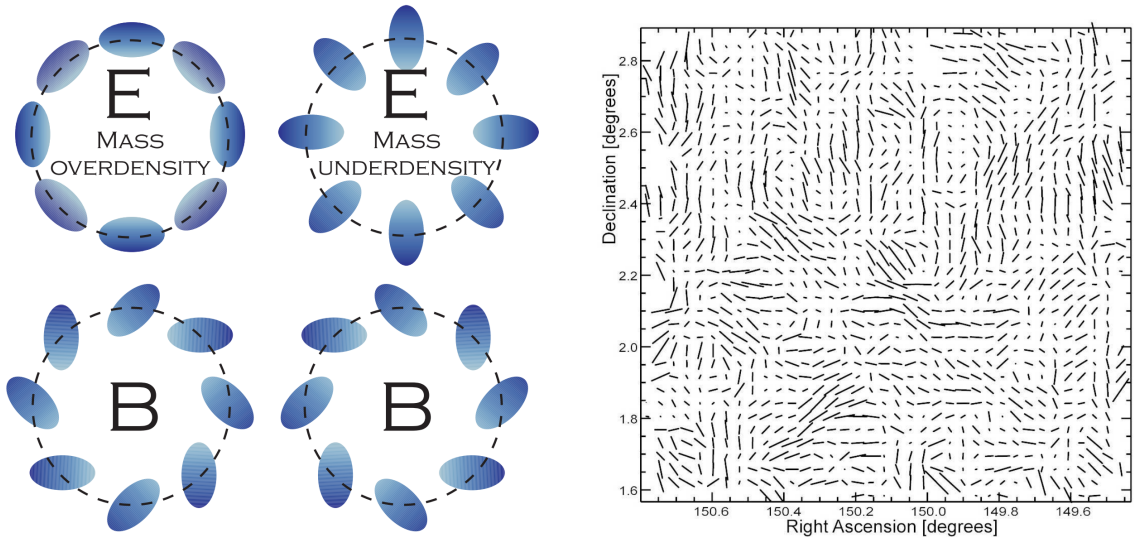


Figure 1-3: Left: Examples of circular “E-mode” and curl-like “B-mode” patterns. Right: The observed ellipticities of half a million distant galaxies within the 2 square degree Hubble Space Telescope COSMOS survey. Reprinted fom Reference [7].

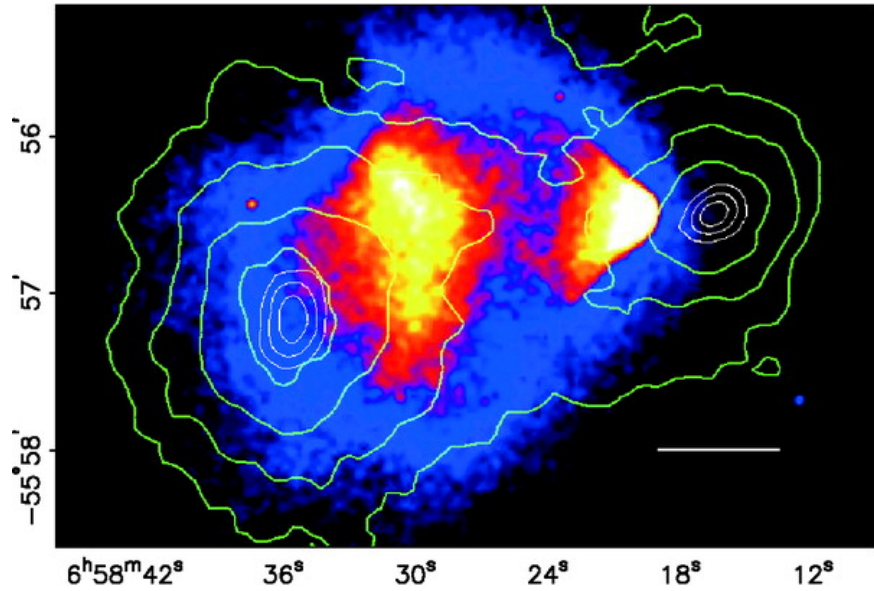


Figure 1-4: The merging cluster 1E0657-558. The green contours show the weak lensing reconstruction of the gravitational potential of the cluster. The colors indicate the X-ray temperature of the plasma, changing from blue to white as the plasma goes from coolest to hottest. The smaller “bullet” cluster on the right which traversed through the larger cluster on the left. Reprinted from Reference [8].

tential of the cluster shown in green contours against temperature color gradient of the X-ray emitting interstellar plasma, it was learned that the gravitational potential of the cluster does not track the dominant baryonic mass contribution coming from the plasma. Instead, the gravitational potential tracks the smaller stellar baryonic mass component. Dark matter must be the dominant gravitational source in the cluster since the center of total mass is offset from the center of baryonic mass. Furthermore, the observation of two gravitational mass centers places strong constraints on the self-interaction of dark matter requiring that the observed mass must have a self-interaction collisional cross section  $\sigma/m < 1.25 \text{ cm}^2 \text{g}^{-1}$  at a 68% confidence level [8].

## 1.2 Relic Density

During the early universe, dark matter (DM) was in thermal equilibrium with the rest of the SM particles with a number density  $n_\chi$  given by

$$n_\chi^{\text{eq}} = \frac{g}{(2\pi)^3} \int f(\vec{p}) d^3\vec{p}, \quad (1.6)$$

where  $g$  is the number of internal degrees of freedom of the DM particle  $\chi$  and  $f(\vec{p})$  is either the Fermi-Dirac or Bose-Einstein distribution, depending on the quantum statistics of the DM particle [9]. At very high temperatures relative to the mass  $m_\chi$  of the DM particle, dark matter and SM particles rapidly convert back and forth with a DM annihilation rate  $\Gamma = \langle \sigma_A v \rangle \cdot n_\chi$ , where  $\langle \sigma_A v \rangle$  is the thermally averaged product of the total cross section for annihilation  $\sigma_A$  and the relative velocity  $v$  of the dark matter particles. After the temperature drops below  $m_\chi$ , the DM annihilation rate  $\Gamma$  drops below the Hubble expansion rate  $H$  of the universe and the DM particles stop annihilating and freeze-out of equilibrium with the SM particles, leaving the DM relic density that we observe today. During the freeze-out process, the time dependence

of the number density  $n_\chi$  is described by the Boltzmann equation [9] as follows

$$\frac{dn_\chi}{dt} + 3Hn_\chi = -\langle\sigma_A v\rangle [(n_\chi)^2 - (n_\chi^{\text{eq}})^2]. \quad (1.7)$$

The term on the left-hand side accounts for the reduction in density due to the expansion of the universe. The two terms on the right-hand side account for the change in density due to annihilation and product of DM particles to and from SM particles, respectively.

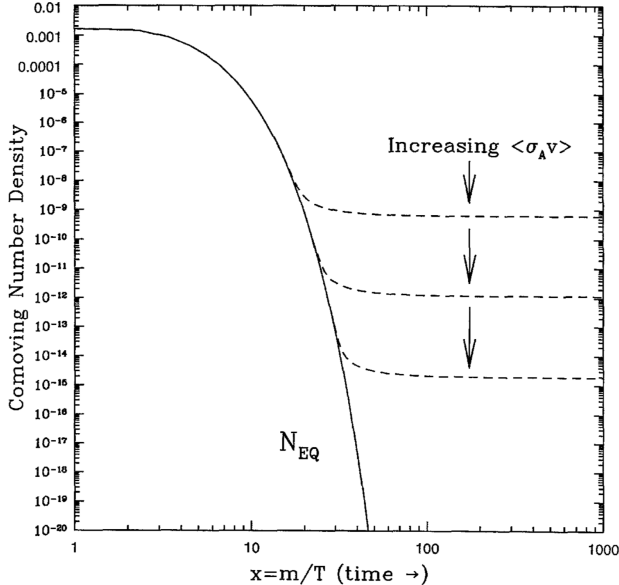


Figure 1-5: Number density of dark matter in the early universe as a function of time. The solid curves are the equilibrium abundance while the dashed curves are the actual abundance after freeze-out. Reprinted from Reference [9].

Figure 1-5 shows the calculated DM number density  $n_\chi$  as a function of time in the early universe. As the annihilation cross section increases, the relic density decreases as the dark matter particles stay in equilibrium longer. Assuming that  $\langle\sigma_A v\rangle$  is independent of energy, an order-of-magnitude estimate of the relic density is given by

$$\Omega_\chi \cdot h^2 = \frac{m_\chi n_\chi}{\rho_c} \simeq \frac{10^{-27} \text{ cm}^3 \text{ s}^{-1}}{\langle\sigma_A v\rangle}, \quad (1.8)$$

where  $h = H_0/(100 \text{ km s}^{-1} \text{ Mpc}^{-1})$  is the reduced Hubble constant and  $\rho_c = 3H^2/(8\pi G)$

is the critical density of the universe [9]. Thus, to first order the DM relic density depends only on two things: the total DM annihilation cross section  $\sigma_A$  and the mass  $m_\chi$  of the DM candidate, as after freeze-out  $T \ll m_\chi$  and the velocity  $v$  is strictly proportional to  $m_\chi$ . The latest Planck results measure that  $\Omega_\chi \cdot h^2 = 0.1200 \pm 0.0012$ , providing strong constraints on the possible values of  $\sigma_A$  and  $m_\chi$ .

### 1.3 Dark Matter Candidates

Dark matter has not been directly observed so far. In the previous sections, we collected all known facts about dark matter to restrict the pool of potential candidates. Any serious dark matter candidate must satisfy the following criteria:

- No or extremely weak interactions with photons, e.g. be **dark**
- Weak baryonic interactions to preserve the DM halos
- Weak self-interactions
- The observed relic density

These four criteria place stringent requirements on dark matter candidates. The light neutrinos, the only SM particles satisfying the first three conditions, are excluded as the total neutrino relic density has a bound of  $\Omega_\nu \cdot h^2 \leq 0.00067$  at 95% confidence level from analysis of the CMB anisotropies. Big Bang Nucleosynthesis and gravitational microlensing have mostly exclude non-luminous baryonic matter from forming the bulk of dark matter. Thus, most theories of dark matter propose a new fundamental particle as a dark matter candidate. The following sections discuss the most common dark matter candidates, namely weakly-interacting massive particles (WIMPs), axions, and sterile neutrinos.

### 1.3.1 Weakly-Interacting Massive Particles

The annihilation cross-section of new particle  $\chi$  with electroweak scale interactions is approximately

$$\langle \sigma_A v \rangle \approx \left( \frac{\alpha \cdot g_\chi^2}{m_\chi} \right)^2 = \left( \frac{e^2}{4\pi} \cdot \frac{(0.8)^2}{100 \text{ GeV}} \right)^2 \simeq 10^{-26} \text{ cm}^3 \text{ s}^{-1}, \quad (1.9)$$

where  $\alpha = e^2/4\pi$  is the fine-structure constant,  $m_\chi = 100 \text{ GeV}$  is the mass of the particle, and  $g_\chi \approx 0.8$  is the effective coupling for the four-point interaction  $\chi\bar{\chi} \rightarrow f\bar{f}$ . Plugging this into Equation 1.8, we obtain  $\Omega_\chi \cdot h^2 \sim 0.1$ , which is very close to the observed value. This numerical coincidence, known as the “WIMP miracle”, motivates a new weakly-interacting massive particle (WIMP) as a good DM candidate [9].

The only criteria to be a WIMP beyond the generic definition of dark matter is that the mass and interaction strength of the new particle must be approximately that of the EWK scale. Thus, a great many new physics models have WIMPs natively, such as the neutralino in supersymmetry and the lightest Kaluza-Klein particle in theories of universal extra dimensions. In this thesis, we shall focus on a set of simplified models that describe WIMP interactions in a relatively model-independent manner so that our results can be reinterpreted in as many theories as possible.

### 1.3.2 Axions

The hypothetical axion particle introduced in Section ?? is a dark matter candidate if the axion decay constant  $f_a$  is large enough as all axion-SM couplings are inversely proportional to it. Constraints from the observed duration of the neutrino burst from supernova SN 1987A require that  $f_a \gtrsim 10^9 \text{ GeV}$  [10], sufficiently high that the axion lifetime exceeds the age of the universe by many orders of magnitude. Thus, the axion is a viable DM candidate due to its long lifetime and weak couplings to SM particles.

After accounting for kinematic mixing with the  $\pi^0$  and  $\eta$  mesons, the axion mass is given by

$$m_a = \left( \frac{\sqrt{m_u m_d}}{m_u + m_d} \right) \left( \frac{f_\pi}{f_a} \right) m_\pi \simeq \left( \frac{10^7 \text{ GeV}}{f_a} \right) \text{ eV}, \quad (1.10)$$

where  $f_\pi$  is the pion decay constant and  $m_u$ ,  $m_d$ , and  $m_\pi$  are the masses of the up quark, the down quark, and the neutral pion, respectively. From this, we see that the axion mass is inversely proportional to  $f_a$ , leading to an upper limit of  $m_a \lesssim 10 \text{ meV}$ . The Planck measurements of the cosmic microwave background also provide a lower (upper) bound on the axion mass  $m_a \gtrsim 10 \mu\text{eV}$  (axion decay constant  $f_a \lesssim 10^{12} \text{ GeV}$ ), otherwise the axion abundance is too high.

The axion obtains a two-photon vertex through loops involving virtual quarks and gluons of the form

$$\mathcal{L}_{a\gamma\gamma} = \frac{1}{4} g_{a\gamma\gamma} \epsilon_{\mu\nu\rho\sigma} F^{\mu\nu} F^{\rho\sigma} a = -g_{a\gamma\gamma} (\vec{E} \cdot \vec{B}) a, \quad (1.11)$$

where  $F^{\mu\nu}$  is the electromagnetic field-strength tensor,  $\vec{E}$  and  $\vec{B}$  are the electric and magnetic fields, respectively, and the coupling constant is

$$g_{a\gamma\gamma} = -\frac{\alpha}{3\pi f_a} \left( \frac{m_u + 4m_d}{m_u + m_d} \right). \quad (1.12)$$

From this, we can see that the axion's coupling to the photon is incredibly small unless in the presence of a strong electromagnetic field. Thus, astrophysical axions are **dark** unless they enter a region with such a field. Searches for axions such as CAST[11] and ADMX[12, 13] exploit this to try to observe axion-to-photon conversions.

### 1.3.3 Sterile Neutrinos

In Section ??, we introduced mass for the SM fermions through the Higgs mechanism in order to preserve  $SU(2)_L$  gauge invariance. However, since the right-handed neutrinos are singlets under the full  $SU(3)_C \times SU(2)_L \times U(1)_Y$  gauge of the SM, it is possible to add explicit Majorana mass terms in addition to the Dirac mass terms in

the SM Lagrangian [14] as follows

$$\begin{aligned}
\mathcal{L}_{\nu_R} &= i\bar{\nu}_R \not{\partial} \nu_R - (\bar{\ell}_L Y_\nu \phi_c \nu_R + \bar{\nu}_R Y_\nu^\dagger \phi_c^\dagger \ell_L) - \frac{1}{2} \left( \bar{\nu}_R^c M_M \nu_R + \bar{\nu}_R M_M^\dagger \nu_R^c \right) \\
&= i\bar{\nu}_R \not{\partial} \nu_R - (\bar{\nu}_L M_\nu \nu_R + \bar{\nu}_R M_\nu^\dagger \nu_L) - \frac{1}{2} \left( \bar{\nu}_R^c M_M \nu_R + \bar{\nu}_R M_M^\dagger \nu_R^c \right) \\
&= i\bar{\nu}_R \not{\partial} \nu_R - \frac{1}{2} \left[ \begin{pmatrix} \bar{\nu}_L & \bar{\nu}_R^c \end{pmatrix} \begin{pmatrix} 0 & M_\nu \\ M_\nu^T & M_M \end{pmatrix} \begin{pmatrix} \nu_L^c \\ \nu_R \end{pmatrix} + h.c. \right], \tag{1.13}
\end{aligned}$$

where  $\nu_R^c$  are the charge conjugates of the right-handed neutrinos,  $h.c.$  stands for hermitian conjugate, and  $Y_\nu$ ,  $M_\nu$ , and  $M_M$  are the Yukawa, Dirac mass, and Majorana mass matrices for the neutrinos, respectively.

In the limit  $M_M \gg M_\nu$ , the combined mass matrix has two distinct sets of eigenvalues: the sterile neutrinos  $\nu_s$  with masses  $m_s \simeq M_M$  and the active neutrinos  $\nu_a$  with masses  $m_a \simeq M_\nu^2/M_M$ . The active and sterile neutrinos are related to the left- and right-handed neutrinos by the active-sterile mixing matrix  $\theta = M_\nu M_M^{-1}$  as follows

$$\begin{aligned}
|\nu_a\rangle &= \cos \theta |\nu_L\rangle + \sin \theta |\nu_R\rangle \\
|\nu_s\rangle &= -\sin \theta |\nu_L\rangle + \cos \theta |\nu_R\rangle. \tag{1.14}
\end{aligned}$$

In this formulation, the active neutrinos are the observed neutrinos of the SM while the sterile neutrino states are a promising dark matter candidate as they only interact with the SM through neutrino oscillations. Furthermore, the sterile neutrinos must have  $m_s \simeq$  keV or else they cannot account for the observed masses of DM-dominated objects without violating the Pauli exclusion principle [15]. Fortunately, this constraint also means that the oscillation rate into active neutrinos is low enough that the sterile neutrino lifetime is longer than the age of the universe. The Majorana mass term also allows for additional CP-violating phases beyond the Dirac phases. Astrophysical detection, accelerator production, and neutrinoless double  $\beta$  decay experiments all place constraints on sterile neutrino properties [16].

## 1.4 Simplified Models for LHC

Without loss of generality, we assume that dark matter consists of a single Dirac fermion WIMP species  $\chi$  with mass  $m_{\text{DM}}$ . In order to observe DM at a hadron collider, there must exist a new mediator particle with mass  $M_{\text{med}}$  that couples to both SM quarks and  $\chi$  with couplings  $g_q$  and  $g_{\text{DM}}$ , respectively. In general, this mediator can have any spin structure; for purposes of simplicity, we limit ourselves to the observed mediators in the SM: a spin-0 scalar  $S$ , a spin-0 pseudoscalar  $P$ , a spin-1 vector  $V_\mu$ , and a spin-1 axial-vector  $A_\mu$  (not to be confused with SM photon).

The Lagrangians for these possible mediators are

$$\mathcal{L}_S = \frac{1}{2}M_{\text{med}}^2 S^2 + g_{\text{DM}} \bar{\chi} S \chi + g_q \sum_q \bar{q} Y_q S q \quad (1.15)$$

$$\mathcal{L}_P = \frac{1}{2}M_{\text{med}}^2 P^2 + g_{\text{DM}} \bar{\chi} \gamma^5 P \chi + i g_q \sum_q \bar{q} Y_q \gamma^5 P q \quad (1.16)$$

$$\mathcal{L}_V = \frac{1}{2}M_{\text{med}}^2 V_\mu V^\mu + g_{\text{DM}} \bar{\chi} \not{V} \chi + g_q \sum_q \bar{q} \not{V} q \quad (1.17)$$

$$\mathcal{L}_A = \frac{1}{2}M_{\text{med}}^2 A_\mu A^\mu + g_{\text{DM}} \bar{\chi} \gamma^5 \not{A} \chi + g_q \sum_q \bar{q} \gamma^5 \not{A} q, \quad (1.18)$$

where  $\{q\}$  and  $\{Y_q\}$  are the SM quarks and their associated Yukawa couplings and we have assumed that the coupling  $g_q$  is universal to all quarks without any loss of generality. The width of the mediators is determined by the coupling constants and mass of the mediator. Thus, these four models are described by only four parameters in addition to the spin structure of their couplings:  $\{g_q, g_{\text{DM}}, m_{\text{DM}}, M_{\text{med}}\}$ . For the results shown in this thesis, we fix  $g_q = 0.25$  and  $g_{\text{DM}} = 1$  to satisfy the narrow width approximation and provide complimentarity to dijet and dilepton searches for new mediators. Meanwhile, we scan the mass parameters  $m_{\text{DM}}$  and  $M_{\text{med}}$  between 1-1000 GeV and 10-2000 GeV, respectively.

As the CMS detector is focused on observing particles through electromagnetic and strong interactions (see Chapter ??), the production of DM particles alone does not result in an observable signature in the detector. Instead, we look for events where

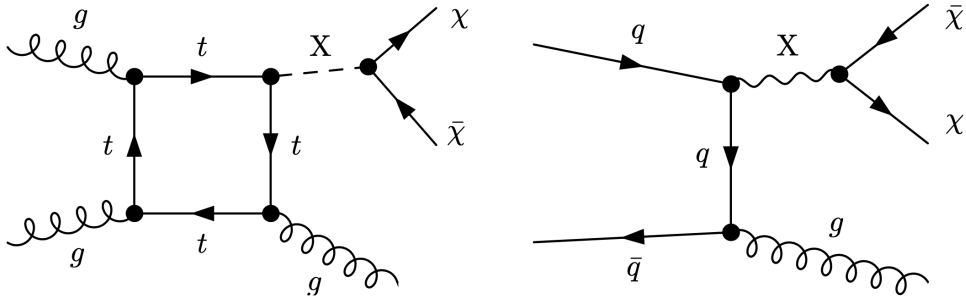


Figure 1-6: Feynmann diagrams for possible dark matter production modes at the LHC, with  $X$  denoting the mediator and  $\chi$  the dark matter particle. The left diagram is most common for scalar and pseudoscalar mediators, while the right diagram is most common for vector and axial mediators. For the right diagram, the gluon can be replaced with any of the EWK gauge boson whereas for the left diagram, other production modes dominate for the EWK gauge bosons. Reprinted from Reference [1].

they are produced in association with a visible SM particle with the resulting signature of the SM particle recoiling against an invisible state. The standard mechanism for producing this final state is for one of the incoming partons to radiate the visible SM particle, usually a quark or a gauge boson, as shown in Figure 1-6. The possible final states split into the categories shown in Table 1.1 with unique final states and interaction strengths.

Name	Strength	Final State
Monojet	$\mathcal{O}(\alpha_s)$	$j + \chi\bar{\chi}$
Monophoton	$\mathcal{O}(\alpha)$	$\gamma + \chi\bar{\chi}$
Mono-Z	$\mathcal{O}(\alpha)/M_Z^2$	$\ell\ell + \chi\bar{\chi}$

Table 1.1: Final states of DM production with approximate interaction strength.

The monojet final state has the highest production rate but also the largest amount of background from SM processes. The Mono-Z final state is the cleanest signature but also has a substantially suppressed production rate due to the mass of the  $Z$  boson and the small branching ratio to leptons. The monophoton final state lands in the middle on both metrics: the production rate is  $\sim 1/10$  that of the monojet final state but also has fewer backgrounds from SM processes. Additionally, the monophoton state has the “advantage” of being able to distinguish between the spin-0 and spin-1 mediators by the “virtue” of the  $gg \rightarrow S\gamma$  and  $gg \rightarrow P\gamma$  processes being forbidden by

Furry's theorem. For the bulk of this thesis, we focus on the monophoton final state, saving comparisons against the monojet and mono- $Z$  states for Chapter ??.

## 1.5 Non-collider Searches

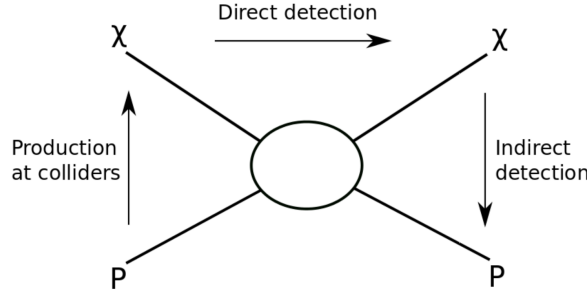


Figure 1-7: Possible dark matter detection channels. Reprinted from Reference [].

The goal of a collider-based search for dark matter is to create pairs of DM candidates through quark-antiquark annihilation, i.e.  $q\bar{q} \rightarrow \chi\bar{\chi}$ . However, there are other ways you can look at this interaction when attempting to find dark matter, as shown in Figure 1-7. The longest running searches for DM particles have been direct detection searches, where one attempts to observe the scattering of a DM particle off of a heavy nucleus, i.e.  $q\chi \rightarrow q\chi$ . Another method involves the inverse process utilized at hadron colliders, the observation of SM particles produced in the annihilation of astrophysical DM pairs, i.e.  $\chi\bar{\chi} \rightarrow q\bar{q}$ . In this section, we shall give a brief overview of the leading experiments for these two approaches.

### 1.5.1 Direct Detection

Direct detection experiments aim to observe a collision between a DM particle  $\chi$  and an atomic nucleus  $N$ . The typical nuclear recoil for such a collision is in the 1–100 keV range and there are various different technologies that are used to identify the recoiling nucleus, as shown in Figure 1-8. The three main signals are light from a scintillating material, charge from an ionization reaction, and phonons from thermal

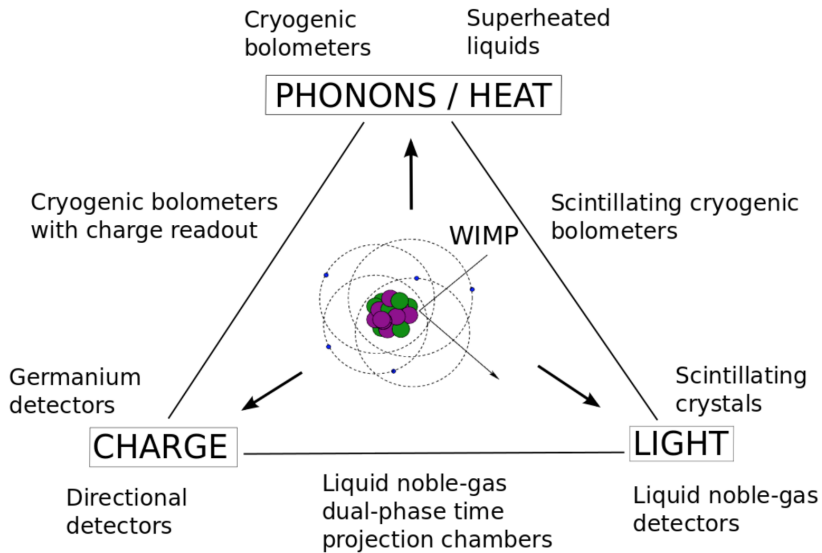


Figure 1-8: Possible signals measured and technologies used in direct detection experiments. Reprinted from Reference [1].

excitations. Many detectors utilize multiple signals in order to enhance background rejection. A final consideration is whether the interaction is spin-independent (SI) or spin-dependent (SD), corresponding to a vector/scalar or axial/pseudoscalar mediator, respectively. The SI DM-nucleus cross-section scales as the number of nucleons squared and thus experiments focusing on SI interactions use materials with a large atomic number. Conversely, the spin-dependent DM-nucleus cross-section depends on the total nuclear spin and experiments focusing on SD interactions use materials with an odd number of nucleons, particularly those with unpaired protons and neutrons. The remainder of this section will discuss three proto-typical direct detection experiments.

The Large Underground Xenon (LUX) experiment is a dual-phase xenon time projection chamber that utilizes both scintillation light and free electrons from ionization to detect nuclear recoils. The active detector volume has 250 kg of ultrapure liquid xenon, a large enough volume that the detector is self-shielding. Odd isotopes make up 47% of naturally occurring xenon, enabling measurements of spin-dependent interactions with approximately half the active detector volume. The latest LUX

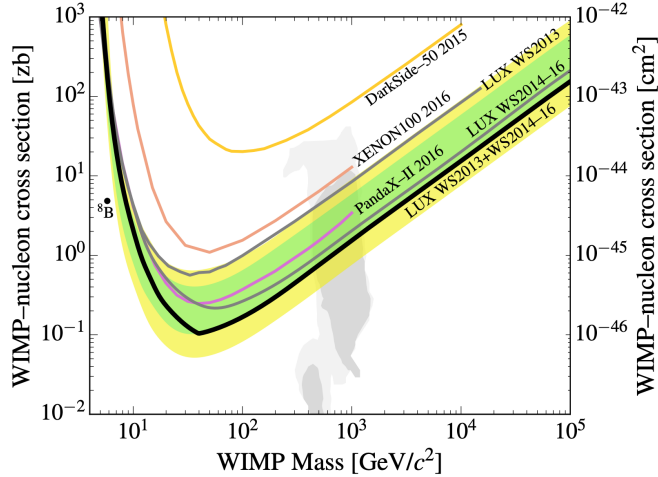


Figure 1-9: Latest SI independent results from the LUX experiment (brazilian flag bands). Reprinted from Reference [1].

results are shown in Figure 1-9.

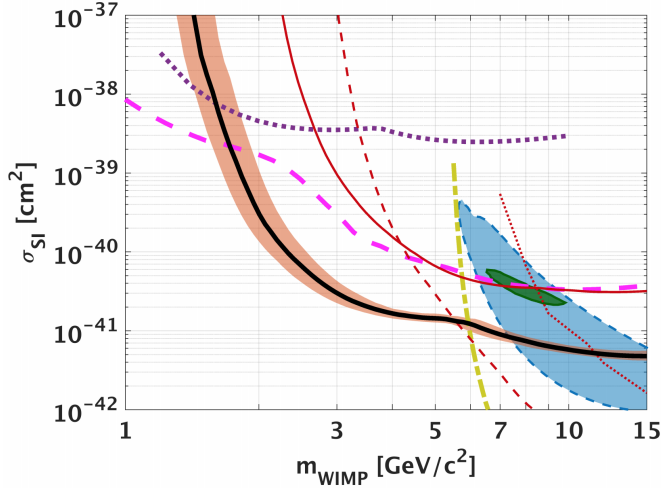


Figure 1-10: Latest SI independent results from the CDMSlite experiment (black line with salmon band). Reprinted from Reference [1].

The CDMSlite experiment uses a cryogenic germanium bolometer that detects phonons and ionization from nuclear recoils. The presence of both signals allows for particle identification, but the most sensitive results only use the phonon signals. CDMSlite is most sensitive to dark matter with masses between 1-10 GeV as shown in Figure 1-10.

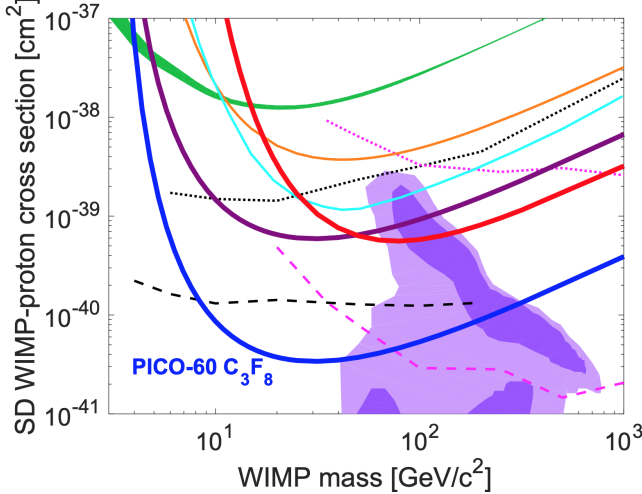


Figure 1-11: Latest SD independent results from the PICO-60 experiment (thick blue line). Reprinted from Reference [].

The PICO-60 experiment uses a bubble chamber filled with  $\text{C}_3\text{F}_8$  to observe nuclear recoils with a threshold of 13.6 keV. This threshold is high enough to reject backgrounds from minimum ionizing particles while still having sufficient signal efficiency. Furthermore, flourine has exactly one unpaired proton and no unpaired neutrons, greatly enhancing the sensitivity to the proton-coupling SD interactions. The latest results from PICO-60 are shown in Figure 1-11.

### 1.5.2 Indirect Detection

In Section 1.2, we discussed the process of dark matter annihilation in the early universe and found that the relic density  $\Omega_\chi \cdot h^2$  depended on the average annihilation cross section  $\langle \sigma_A v \rangle$ . In Section 1.3.1, we found that a 100 GeV WIMP particle must have  $\langle \sigma_A v \rangle \sim 10^{-26} \text{ cm}^3 \text{ s}^{-1}$  in order to produce the observed relic density. While our calculation in Section 1.2 assumed that the DM number density didn't change appreciably after freezeout, there is still a non-zero annihilation rate of  $n_\chi^2 \langle \sigma_A v \rangle / 2$  for dark matter to SM particles. With this decay rate and the observed relic density, there should be  $\mathcal{O}(10)$  particles from DM annihilation reaching Earth per year per square meter. Thus, it is possible to learn about dark matter by observing the particle flux near Earth.

While dark matter can decay to a pair of any SM particles, the only ones that live long enough to reach Earth are photons, neutrinos, electrons, positrons, protons, and anti-protons, whether produced directly or from decays of short-lived particles. While it is possible to measure the flux of all of these particles, it is only possible to observe the energy spectrum and source locations of photons and neutrinos as galactic magnetic fields obscure these for the charge particles. Thus, experiments such as the Alpha Magnetic Spectrometer (AMS-02) look for a rise in the positron and anti-proton fractions of the cosmic ray flux to find signs of WIMP annihilation. Similarly, gamma ray telescopes such as the Fermi Large Area Telescope (Fermi-LAT) search for high-energy photons originating from dwarf spheroidal galaxies as they have especially high ratios of dark matter to luminous matter. Both experiments have tentative signals that are yet to be confirmed.

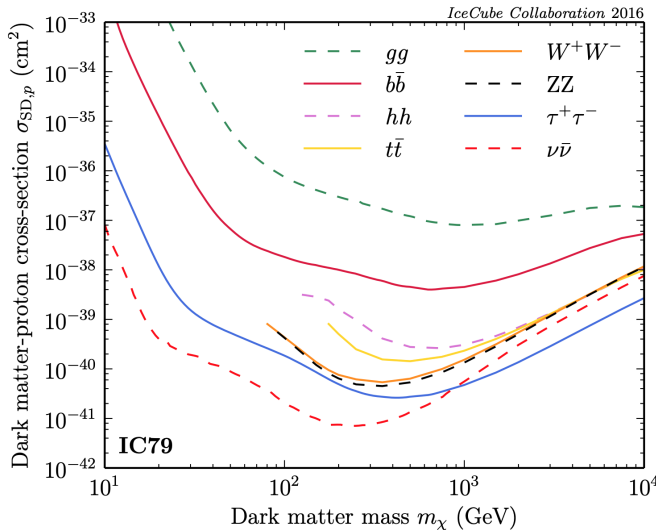


Figure 1-12: Latest SD independent results from the IceCube experiment. Reprinted from Reference [1].

The neutrino channel differs from the other two because it is sensitive to the annihilation of WIMPs that have been gravitationally captured by the sun. While solar WIMPs can decay to any SM particle, only neutrinos are capable of escaping the sun. Furthermore, astrophysical uncertainties are very small for neutrinos originating from the sun versus galactic sources. Additionally, solar WIMPs are in equilibrium, so the annihilation flux depends on the DM-nucleon cross-section instead of the annil-

ihilation cross-section allowing for easy comparison with direct detection experiments. Since the sun consists primarily of hydrogen, observations of solar WIMPs are especially sensitive to spin-dependent processes. The IceCube neutrino observatory is a Cherenkov light detector consisting of a cubic kilometer of Antarctic ice instrumented with 79 strings of photomultiplier tubes. Figure 1-12 shows the latest results from IceCube, with each curves assuming annihilation into a different SM particle pair.

## 1.6 Summary

Copious astrophysical evidence exists for a non-relativistic non-baryonic type of matter referred to as dark matter that constitutes  $\sim 27$  of the energy of the universe. The favored source for dark matter is a new beyond the Standard Model particle that has weak interactions with photons, baryons, and itself and a relic density of  $\Omega_\chi \cdot h^2 = 0.1200 \pm 0.0012$ . While other candidates exist, a new weakly-interacting massive particle is a dark matter candidate found in many theories of new physics. Collider, direct detection, and indirect detection searches can all be interpreted in the context of simplified models, which posit a new Dirac fermion DM particle and a massive mediator. The remainder of this thesis focuses on a search for dark matter produced in conjunction with a single photon at the Large Hadron Collider using the Compact Muon Solenoid detector.



# Bibliography

- <sup>1</sup>J. J. Condon and A. M. Matthews, “ $\Lambda$ CDM cosmology for astronomers”, Publications of the Astronomical Society of the Pacific **130**, 073001 (2018).
- <sup>2</sup>M. Roos, “Dark Matter: The evidence from astronomy, astrophysics and cosmology”, arXiv e-prints, arXiv:1001.0316, arXiv:1001.0316 (2010).
- <sup>3</sup>F. Zwicky, “Die Rotverschiebung von extragalaktischen Nebeln”, Helvetica Physica Acta **6**, 110–127 (1933).
- <sup>4</sup>G. D’Amico, M. Kamionkowski, and K. Sigurdson, “Dark Matter Astrophysics”, arXiv e-prints, arXiv:0907.1912, arXiv:0907.1912 (2009).
- <sup>5</sup>V. C. Rubin, W. K. Ford Jr., and N. Thonnard, “Rotational properties of 21 SC galaxies with a large range of luminosities and radii, from NGC 4605 /R = 4kpc/ to UGC 2885 /R = 122 kpc/”, **238**, 471–487 (1980).
- <sup>6</sup>A. H. Broeils, K. G. Begeman, and R. H. Sanders, “Extended rotation curves of spiral galaxies: dark haloes and modified dynamics”, Monthly Notices of the Royal Astronomical Society **249**, 523–537 (1991).
- <sup>7</sup>R. Massey, T. Kitching, and J. Richard, “The dark matter of gravitational lensing”, Reports on Progress in Physics **73**, 086901 (2010).
- <sup>8</sup>D. Clowe, M. Bradač, A. H. Gonzalez, M. Markevitch, S. W. Randall, C. Jones, and D. Zaritsky, “A direct empirical proof of the existence of dark matter”, The Astrophysical Journal **648**, L109–L113 (2006).
- <sup>9</sup>G. Jungman, M. Kamionkowski, and K. Griest, “Supersymmetric dark matter”, Physics Reports **267**, 195–373 (1996).

- <sup>10</sup>G. G. Raffelt, “Astrophysical axion bounds”, in *Axions: theory, cosmology, and experimental searches*, edited by M. Kuster, G. Raffelt, and B. Beltrán (Springer Berlin Heidelberg, Berlin, Heidelberg, 2008), pp. 51–71.
- <sup>11</sup>V. Anastassopoulos et al., “New CAST Limit on the Axion-Photon Interaction”, *Nature Phys.* **13**, 584–590 (2017).
- <sup>12</sup>N. Du, N. Force, R. Khatiwada, E. Lentz, R. Ottens, L. J. Rosenberg, G. Rybka, G. Carosi, N. Woollett, D. Bowring, A. S. Chou, A. Sonnenschein, W. Wester, C. Boutan, N. S. Oblath, R. Bradley, E. J. Daw, A. V. Dixit, J. Clarke, S. R. O’Kelley, N. Crisosto, J. R. Gleason, S. Jois, P. Sikivie, I. Stern, N. S. Sullivan, D. B. Tanner, and G. C. Hilton, “Search for invisible axion dark matter with the axion dark matter experiment”, *Phys. Rev. Lett.* **120**, 151301 (2018).
- <sup>13</sup>C. Boutan, M. Jones, B. H. LaRoque, N. S. Oblath, R. Cervantes, N. Du, N. Force, S. Kimes, R. Ottens, L. J. Rosenberg, G. Rybka, J. Yang, G. Carosi, N. Woollett, D. Bowring, A. S. Chou, R. Khatiwada, A. Sonnenschein, W. Wester, R. Bradley, E. J. Daw, A. Agrawal, A. V. Dixit, J. Clarke, S. R. O’Kelley, N. Crisosto, J. R. Gleason, S. Jois, P. Sikivie, I. Stern, N. S. Sullivan, D. B. Tanner, P. M. Harrington, and E. Lentz, “Piezoelectrically tuned multimode cavity search for axion dark matter”, *Phys. Rev. Lett.* **121**, 261302 (2018).
- <sup>14</sup>M. Drewes, “The Phenomenology of Right Handed Neutrinos”, *Int. J. Mod. Phys. E* **22**, 1330019 (2013).
- <sup>15</sup>A. Boyarsky, O. Ruchayskiy, and M. Shaposhnikov, “The role of sterile neutrinos in cosmology and astrophysics”, *Annual Review of Nuclear and Particle Science* **59**, 191–214 (2009).
- <sup>16</sup>A. Boyarsky, M. Drewes, T. Lasserre, S. Mertens, and O. Ruchayskiy, “Sterile neutrino dark matter”, *Progress in Particle and Nuclear Physics* **104**, 1–45 (2019).